

Qualitative and Numerical Analysis of a Cosmological Model Based on an Asymmetric Scalar Doublet with Minimal connections.

IV. Numerical Modeling and Types of Behavior of the Model

Yu. G. Ignat'ev and I. A. Kokh

N. I. Lobachevsky Institute of Mathematics and Mechanics of Kazan Federal University,
Kremleovskaya str., 35, Kazan, 420008, Russia.

Abstract

On the basis of a qualitative and numerical analysis of a cosmological model based on an asymmetric scalar doublet of nonlinear, minimally interacting scalar fields – one classical and one phantom, peculiarities of the behavior of the model near zero energy hypersurfaces have been revealed. Numerical models have been constructed, in which the dynamical system has limit cycles on the zero-energy hypersurfaces. Three types of behavior of the cosmological model have been distinguished, configured by the fundamental constants of the scalar fields and the initial conditions. It is shown that over a wide sector of values of the fundamental constants and initial conditions, the cosmological models have a tendency to adhere to the zero-energy hypersurfaces corresponding to 4-dimensional Euclidean space.

Keywords: cosmological model, phantom scalar field, classical scalar field, asymmetric scalar doublet, qualitative analysis, numerical modeling, Euclidean limit cycles.

1 Introduction

In our previous papers [1–3] we presented a qualitative analysis of a cosmological model, based on an asymmetric scalar doublet, and an analytical and numerical study of its behavior near zero effective energy hypersurfaces. In [3] we also introduced maps of singular points of a dynamical system described by a normal autonomous system of ordinary differential equations [1]:

$$\begin{aligned}\Phi' &= Z, \\ Z' &= -\sqrt{3}Z\sqrt{\left(Z^2 + e\Phi^2 - \frac{\alpha_m}{2}\Phi^4\right) - \left(z^2 - \varepsilon\mu^2\varphi^2 + \frac{\beta_m}{2}\varphi^4\right) + \lambda_m - e\Phi + \alpha_m\Phi^3}, \\ \varphi' &= z,\end{aligned}\tag{1}$$

$$z' = -\sqrt{3}z\sqrt{\left(Z^2 + e\Phi^2 - \frac{\alpha_m}{2}\Phi^4\right) - \left(z^2 - \varepsilon\mu^2\varphi^2 + \frac{\beta_m}{2}\varphi^4\right) + \lambda_m + \varepsilon\mu^2\varphi - \beta_m\varphi^3},$$

where

$$\alpha_m = \frac{\alpha}{m^2}, \quad \beta_m = \frac{\beta}{m^2}, \quad \lambda_m = \frac{\lambda}{m^2}, \quad \Lambda_m = \lambda_m - \frac{1}{2\alpha_m} - \frac{\mu^2}{2\beta_m}, \quad \text{and} \quad \mu \equiv \frac{m}{m}$$

are normalized, dimensionless parameters of the model, which we will assign in the form of a list \mathbf{P}

$$\mathbf{P} \equiv [\alpha_m, \beta_m, e, \varepsilon, \mu, \lambda_m], \quad \mathbf{I} \equiv [\Phi(0), Z(0), \varphi(0), z(0)],\tag{2}$$

with \mathbf{I} being a list of initial conditions¹.

¹ Since system (1) is invariant with respect to shifts of dimensionless time τ , the choice of the initial time $\tau_0 = 0$ has no meaning.

In the present paper, we carry out a detailed numerical study of the cosmological evolution of an asymmetric scalar doublet as a function of the parameters of the model, taking into account the results of the previous qualitative analysis. Note that the Hubble constant $H(t)$ and the invariant cosmological acceleration Ω are assigned by the formulas [3]²

$$H(t) = \frac{\dot{a}}{a} \geq 0, \quad \Omega(t) = \frac{a\ddot{a}}{\dot{a}^2} \equiv 1 + \frac{\dot{H}}{H^2} = -\frac{1}{2}(1 + 3\kappa), \quad (3)$$

where $\kappa = p_m/\mathcal{E}_m$ is the ratio of the effective pressure to the effective energy density – it is the effective barotropic coefficient, and the effective energy density and pressure of the dynamical system have the form

$$\begin{aligned} \mathcal{E}_m(\Phi, Z, \varphi, z) &\equiv \left(Z^2 + e\Phi^2 - \frac{\alpha_m}{2}\Phi^4 \right) + \left(-z^2 + \varepsilon\mu^2\varphi^2 - \frac{\beta_m}{2}\varphi^4 \right) + \lambda_m, \\ p_m(\Phi, Z, \varphi, z) &\equiv \left(Z^2 - e\Phi^2 + \frac{\alpha_m}{2}\Phi^4 \right) - \left(z^2 + \varepsilon\mu^2\varphi^2 - \frac{\beta_m}{2}\varphi^4 \right) - \lambda_m. \end{aligned}$$

2 Numerical modeling of the dynamical system: $\lambda = 0$

We present results of a numerical integration demonstrating the indicated peculiarities. We note at once that the large number of parameters of the cosmological model based on an asymmetric doublet – there are six of them in all – makes sorting through all of the possible variants an extremely cumbersome task; therefore, we present only a few results below – those which we think are the most interesting.

2.1 Case of accessibility of all singular points

$$\mathbf{P} = [1, 1, 1, 1, 1, 0]. \quad (4)$$

2.1.1 General properties of the phase space

In this case, the singular points have the following coordinates:

$$\begin{aligned} M_0(0, 0, 0, 0); \quad M_{01}(1, 0, 0, 0); \quad M_{02}(-1, 0, 0, 0), \\ M_{10}(0, 0, 1, 0); \quad M_{20}(0, 0, -1, 0); \quad M_{11}(1, 0, 1, 0), \\ M_{12}(1, 0, -1, 0); \quad M_{21}(-1, 0, 1, 0); \quad M_{22}(-1, 0, -1, 0), \end{aligned} \quad (5)$$

and the invariant characteristics σ_i^2 are equal to [3]

$$\sigma_1^2 = \frac{3}{8}, \quad \sigma_2^2 = \frac{3}{8}, \quad \sigma_3^2 = \frac{3}{4}.$$

All nine singular points of the dynamical system are accessible. The character of these points was represented in the scheme presented in Fig. 1 of [3]. The dependence of the boundaries of the forbidden regions of phase space in the projections Σ_Φ and Σ_φ on the values of the dual potentials is shown in Fig. 1.

Although the case under consideration is quite standard and does not contain any interesting features in the behavior of the model, we shall consider it in more detail in order to demonstrate general properties of the asymmetric scalar doublet model.

² Note that the condition $H \geq 0$, employed in our work, as shown in [4], can be lifted, at least for the case of an isolated classical field with a nonminimal interaction.

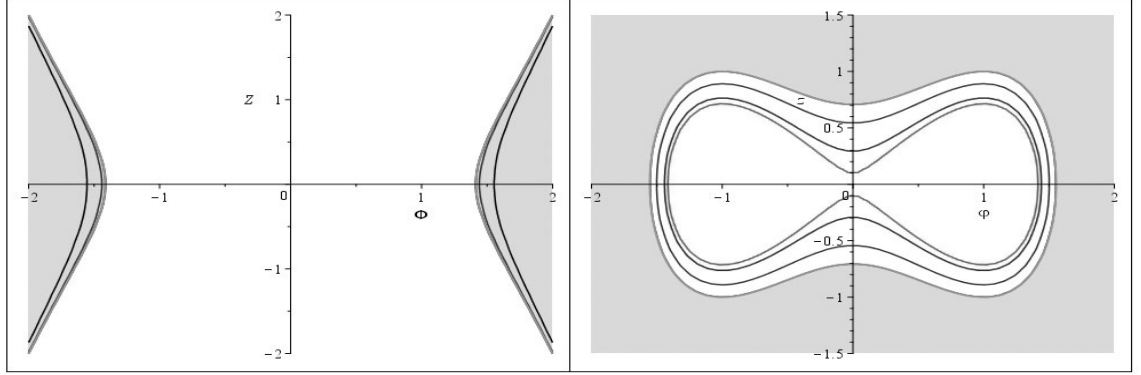


Figure 1: Dependence of the forbidden region (indicated by the light-gray color) in the projections Σ_Φ (left) and Σ_φ (right) on the values of the dual potentials for the model parameters listed in Eq. (4): left – from the interior curves to the exterior curves: $\varphi = 0.01, 0.1, 0.3$ and 1 , the interior regions are forbidden, right – from the interior curves to the exterior curves: $\Phi = 0.1, 0.3, 0.6$ and 1 , the exterior regions are forbidden.

2.1.2 Phase trajectories of the dynamical system

Figures 2–5 present the results of numerical modeling of dynamical system (1) for the model parameters listed in Eq. (4) and the initial conditions

$$\mathbf{I} = [0.7, 0.5, 0.01, 0]. \quad (6)$$

Here and below, the circles correspond to the beginning and end of a phase trajectory, and the x's mark the singular points. It can be seen in Fig. 2 that the phase trajectories in the $\{\Phi, Z\}$ plane rebound from the saddle points M_{10} and M_{20} and then spiral around the attractive focus M_0 . Simultaneously with this, the phase trajectories in the $\{\varphi, z\}$ plane rebound from the saddle point M_0 and then spiral around the attractive foci M_{01} and M_{02} (Fig. 3). This situation becomes clearer in the phase diagram in the plane of singular points $\{\Phi, \varphi\}$ (Fig. 4). Thus, the numerical results confirm the conclusions of the qualitative theory presented in the map of singular points in Fig. 1 of [3].

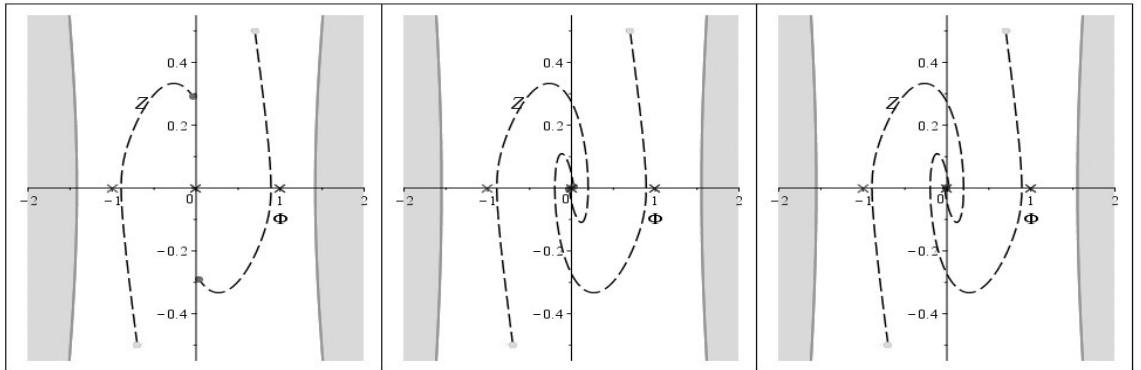


Figure 2: Cosmological evolution of a scalar doublet with the parameters listed in Eq. (4) and the initial conditions listed in Eq. (6) in the *classical* plane $\Sigma_\Phi \equiv \{\Phi, Z\}$. The phase diagrams correspond to the times (from left to right) $\tau = 5, 10$ and 20 . The forbidden regions correspond to the final time.

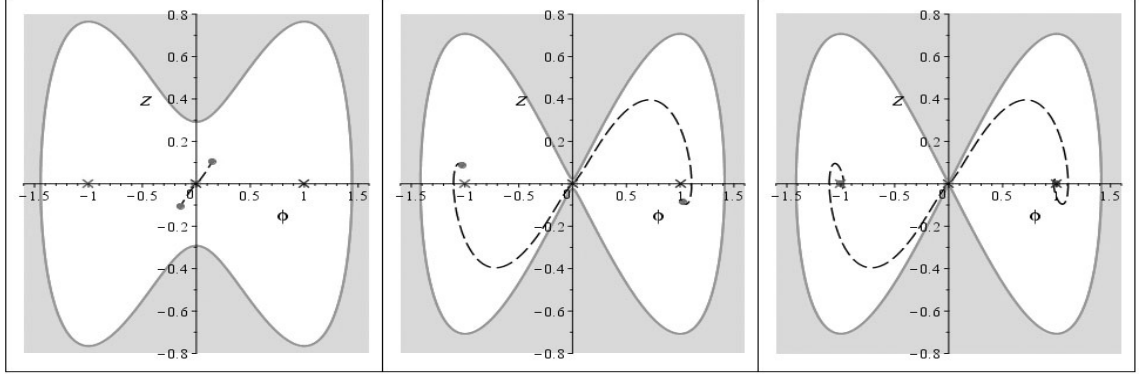


Figure 3: Cosmological evolution of a scalar doublet with the parameters listed in Eq. (4) and the initial conditions listed in Eq. (6) in the *phantom* plane $\Sigma_\varphi \equiv \{\varphi, z\}$. The phase diagrams correspond to the times (from left to right) $\tau = 5, 10$ and 20 . The forbidden regions correspond to the final time.

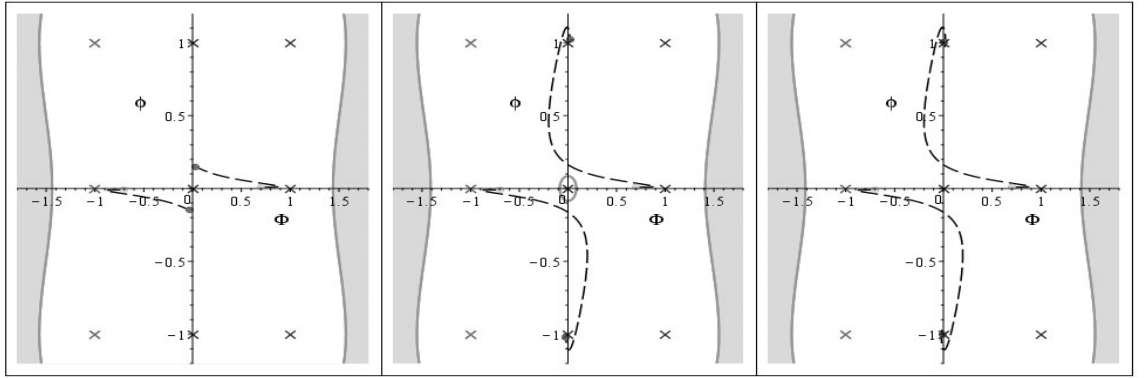


Figure 4: Cosmological evolution of a scalar doublet with the parameters listed in Eq. (4) and the initial conditions listed in Eq. (6) in the plane of potentials $\{\Phi, \varphi\}$. The phase diagrams correspond to the times (from left to right) $\tau = 5, 10$ and 20 .

Figure 5 depicts the evolution of the physical characteristics of the cosmological model with the parameters listed in Eq. (4). Note that, according to the generally accepted classification, \varkappa takes the value $\varkappa = 0$ for nonrelativistic matter (in this case $\Omega = -1/2$), $\varkappa = 1/3$ for ultrarelativistic matter (in this case $\Omega = -1$), $\varkappa = -1/3$ for quintessence (in this case $\Omega = 0$), $\varkappa = -1$ for pure inflation (in this case $\Omega = +1$), and $\varkappa < -1$ for dark energy (in this case $\Omega > +1$). As can be seen from Fig. 5, all of these values in the case under consideration after a burst tend toward constant values, and $\mathcal{E}_m + p_m \rightarrow 0$ as $\tau \rightarrow 0$, which corresponds to inflation in the final stage of evolution. Thus, the case under consideration is very close to the standard scenario with only one difference, namely that late inflation is supported by a phantom field, not a classical one.

The scenario considered above corresponds to small initial values of the phantom potential $\varphi(0) = \pm 0.01$. An increase in the initial value of the phantom potential can substantially alter the cosmological scenario. Let us specify the initial position of the dynamical system above the singular point M_{01} :

$$\mathbf{I} = [0.9, 0.5, 1.3, 0.5]. \quad (7)$$

In this case, we obtain phase diagrams that are fundamentally different from those considered above (Figs.

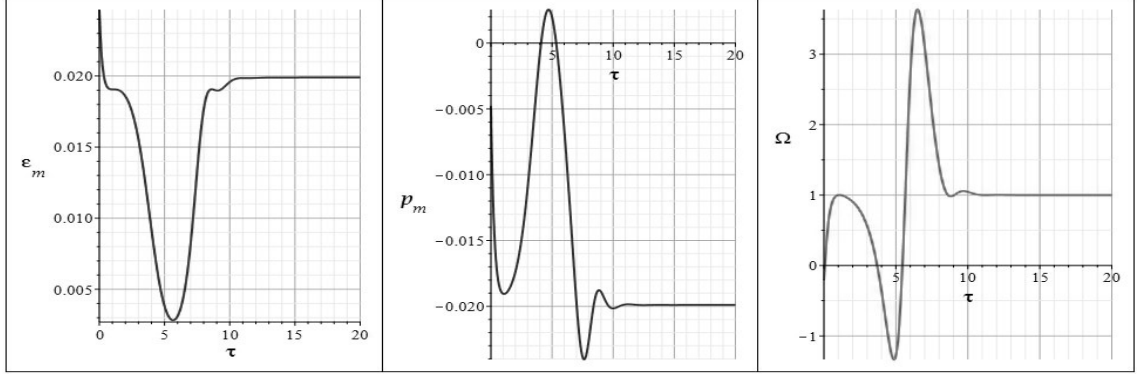


Figure 5: Cosmological evolution of the physical characteristics of the cosmological model with the parameters listed in Eq. (4) and the initial conditions listed in Eq. (6). From left to right: the dimensionless effective energy \mathcal{E}_m , the dimensionless effective pressure p_m , and the invariant cosmological acceleration Ω .

6–8): the phase trajectories circumvent singular points of the type *saddle/focus* and asymptotically press down upon the boundaries of the forbidden region.

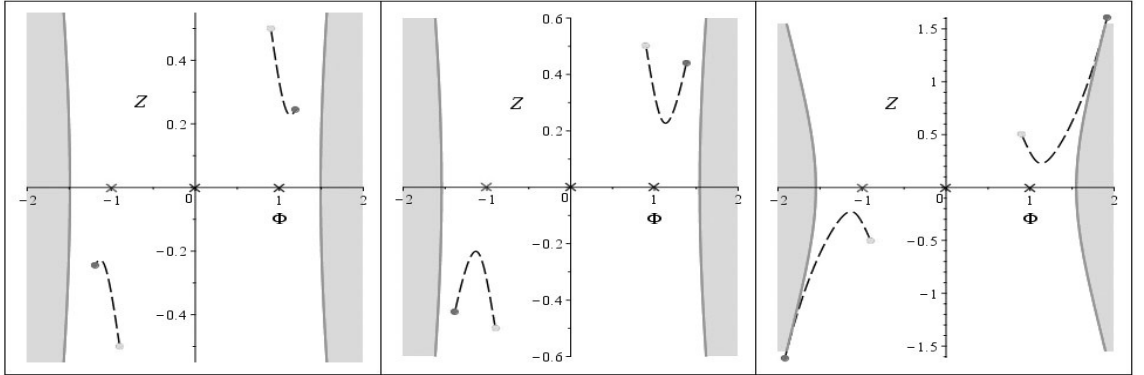


Figure 6: Cosmological evolution of a scalar doublet with the parameters listed in Eq. (4) and the initial conditions listed in Eq. (7) in the *classical* plane $\Sigma_\Phi \equiv \{\Phi, Z\}$. The phase diagrams correspond to the times (from left to right) $\tau = 1, 2$ and 2.2489 .

Next, for simultaneous imaging of unlike-scale and unlike-sign quantities, we shall make use of a one-to-one, continuously differentiable function which we devised $\text{Lig}(x)$:

$$\text{Lig}(x) \equiv \text{sgn}(x) \log(1 + |x|),$$

which is such that

$$\text{Lig}(x) \approx \begin{cases} x, & |x| \rightarrow 0, \\ \text{sgn}(x) \log |x|, & |x| \rightarrow \infty. \end{cases}$$

Figure 9 depicts the evolution of the physical characteristics of the cosmological model with the parameters listed in Eq. (4) and the initial conditions listed in Eq. (7). We see that the effective energy tends rapidly to zero, the pressure becomes positive, and the invariant cosmological acceleration tends to infinitely large negative values. Thus, there takes place a total and abrupt cessation of cosmological expansion, and the Universe becomes Euclidean. The above examples show how different the behavior of the cosmological model

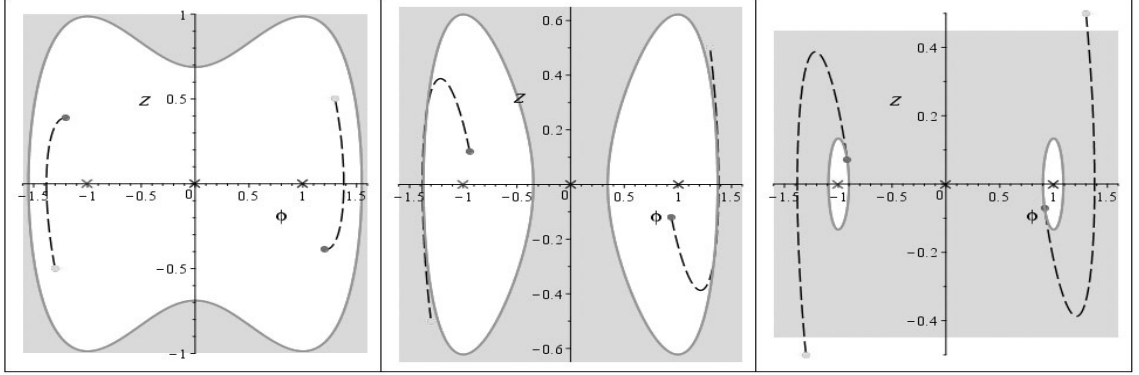


Figure 7: Cosmological evolution of a scalar doublet with the parameters listed in Eq. (4) and the initial conditions listed in Eq. (7) in the *phantom* plane $\Sigma_\varphi \equiv \{\varphi, z\}$. The phase diagrams correspond to the times (from left to right) $\tau = 1, 2$ and 2.2489 .

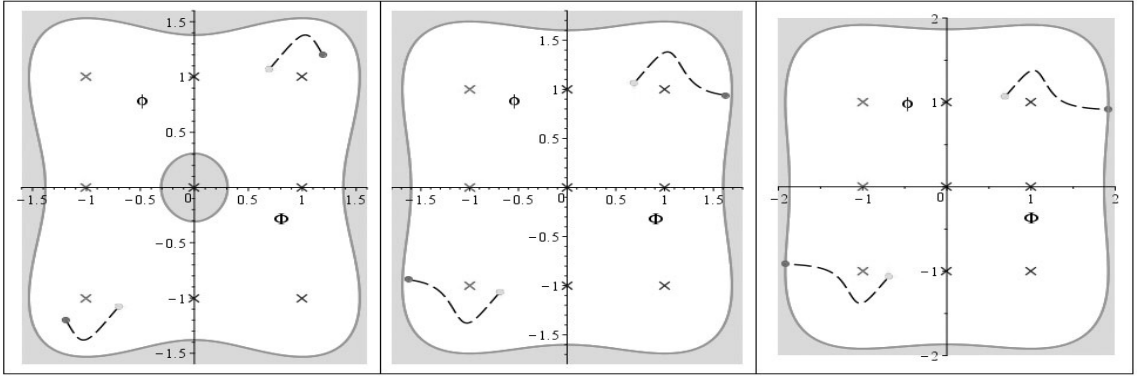


Figure 8: Cosmological evolution of a scalar doublet with the parameters listed in Eq. (4) and the initial conditions listed in Eq. (7) in the plane of the potentials $\{\Phi, \varphi\}$. The phase diagrams correspond to the times (from left to right) $\tau = 1, 2$ and 2.2489 .

can be, depending on its initial position relative to the singular points. Note that the results shown in Fig. 9 describe the case of the transition of the inflationary Universe to a Euclidean one. As we see, no Big Rip problem arises in our model.

2.1.3 Influence of the values of the parameters of the model

Let us elucidate how the absolute values of the parameters α_m and β_m , with the signs of all the parameters unchanged, influence the behavior of the model. As an example, let us consider the case

$$\mathbf{P} = [10, 10, 1, 1, 1, 0]. \quad (8)$$

The map of the singular points in this example coincides with the map in Fig. 1 [3] if we make the substitution $1 \rightarrow 1/\sqrt{10}$ in the coordinates. Figures 10–12 present results of a numerical modeling of dynamical system (1) for the parameters of the model listed in Eq. (4) and the initial conditions listed in Eq. (9) corresponding the initial values of the potentials:

$$\mathbf{I} = [0.3, 0, 0.01, 0]. \quad (9)$$

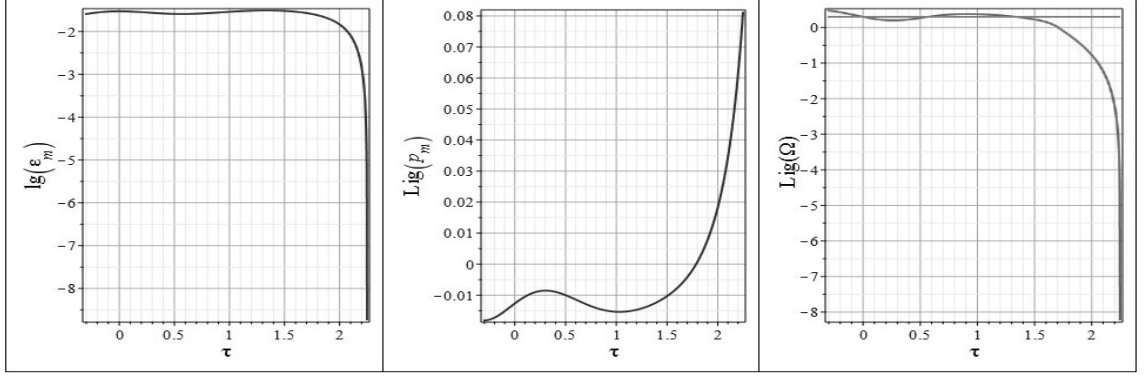


Figure 9: Cosmological evolution of the physical characteristics of the cosmological model with the parameters listed in Eq. (4) and the initial conditions listed in Eq. (7). From left to right: the dimensionless effective energy $\log(\mathcal{E}_m)$, the dimensionless effective pressure $\text{Lig}(p_m)$, and the invariant cosmological constant $\text{Lig}(\Omega)$. The gray horizontal line in the middle of the graph corresponds to the value $\Omega = 1$, i.e., to inflation.

It is easy to see that this case does not differ qualitatively from the case considered above with the parameters listed in Eq. (4) (see Figs. 2–5). The change in the initial conditions leads to analogous results. The main factor here is accessibility of all the singular points.

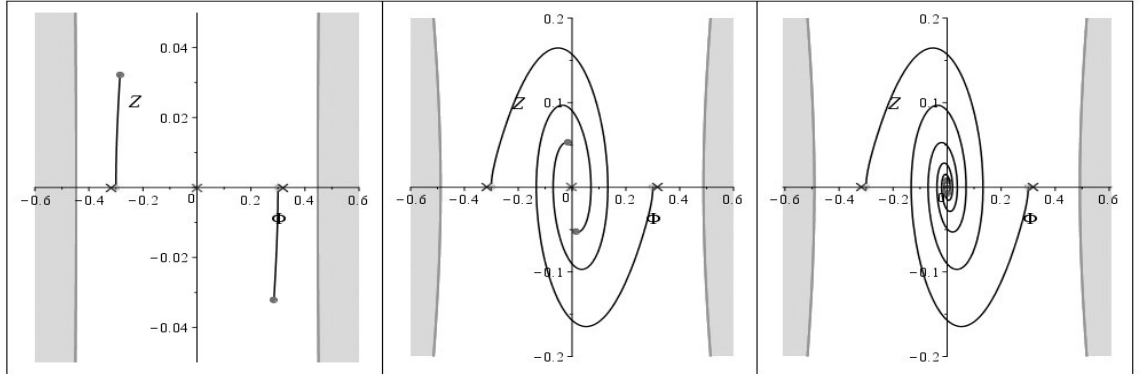


Figure 10: Cosmological evolution of the scalar doublet with the parameters listed in Eq. (4) and the initial conditions listed in Eq. (9) in the *classical* plane $\Sigma_\Phi \equiv \{\Phi, Z\}$. The phase diagrams correspond to the times (from left to right) $\tau = 5, 10$ and 20 . The forbidden regions correspond to the final time.

2.2 Bursts of cosmological acceleration

As was noted in [7–9], the presence of a phantom field in the cosmological model for small values of the potential of the phantom field leads to the appearance of phantom bursts of super-acceleration, characterized by large values of Ω . Figure 13 shows such bursts. As we see, with decrease of the initial value of the phantom field potential, the burst of acceleration takes place at a later time with simultaneous growth of its amplitude. After the burst, the model enters the inflation stage.

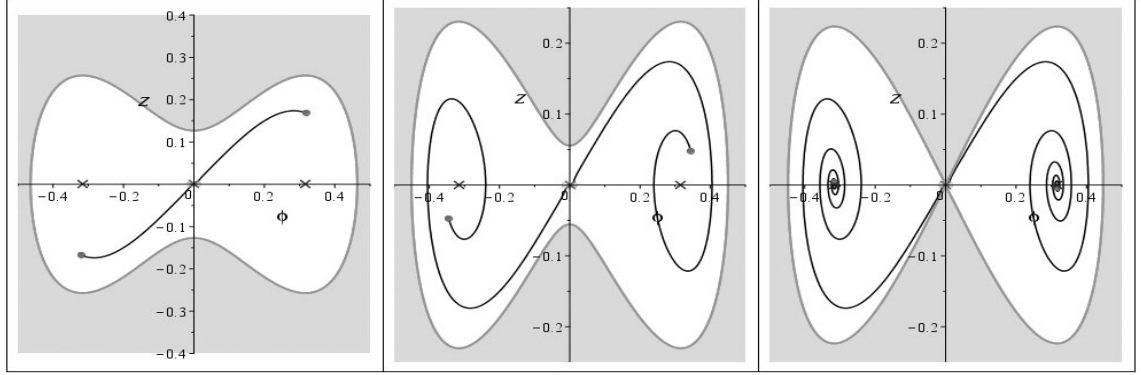


Figure 11: Cosmological evolution of a scalar doublet with the parameters listed in Eq. (4) and the initial conditions listed in Eq. (9) in the phantom plane $\Sigma_\varphi \equiv \{\varphi, z\}$.

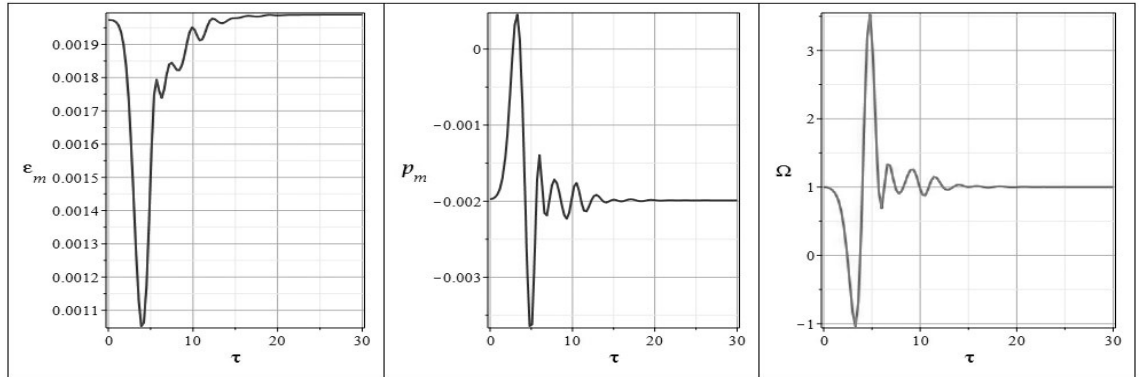


Figure 12: Cosmological evolution of the physical characteristics of the cosmological model with the parameters listed in Eq. (4) and the initial conditions listed in Eq. (9). From left to right: the dimensionless effective energy \mathcal{E}_m , the dimensionless effective pressure p_m , and the invariant cosmological acceleration Ω .

3 Analysis of the results

As our investigations have shown, dynamical system (1) can have three types of behavior:

I. Standard. The phase trajectories in both planes, Σ_Φ and Σ_φ , spiral around and onto the centers/foci. This case can be broken down into three subcases:

1. The phase trajectories in both planes wind around and onto the accessible zero center M_0 . This case corresponds to the parameters listed in Eq. (10) and the initial conditions listed in Eq. (11). Here the pressure of the dynamical system tends to zero and the cosmological acceleration executes oscillations with amplitude on the order of 1 near the value $\Omega_0 = -1/2$, corresponding to the nonrelativistic equation of state.

2. The phase trajectories in the *classical* plane wind around and onto the accessible nonzero focus M_0 , whereas the phase trajectories in the phantom plane wind around and onto the accessible nonzero foci M_{01} and M_{02} . This case corresponds, for example, to the parameters listed in Eq. (4) and the initial conditions listed in Eq. (6) (see Figs. 3–6); to the parameters listed in Eq. (4) and the initial conditions listed in Eq. (9) (see Figs. 11–13). In all of these cases, the magnitude of the cosmological acceleration has a jump $\Omega_{\max} > 1$, after which the cosmological model enters the inflationary regime $\Omega = 1$.

3. The phase trajectories in the *classical* plane wind around and onto the inaccessible nonzero centers/foci

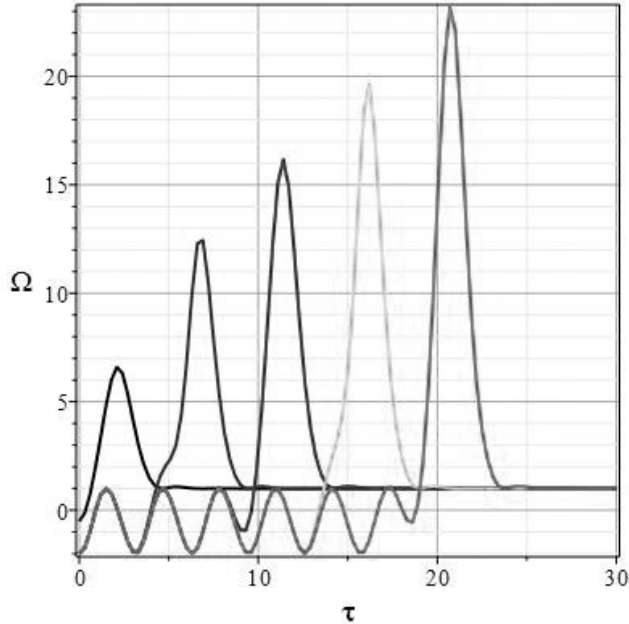


Figure 13: Bursts of cosmological acceleration Ω for the parameters of the model listed in Eq. (4) for the initial value of the potential of the classical field and its derivative $\Phi(0) = 0.1$, $Z(0) = 0$, $z(0) = 0$. From left to right: $\varphi(0) = 10^{-1}$, $\varphi(0) = 10^{-3}$, $\varphi(0) = 10^{-5}$, $\varphi(0) = 10^{-7}$ and $\varphi(0) = 10^{-9}$.

M_{10} and M_{20} , whereas the phase trajectories in the phantom plane wind around and onto the inaccessible nonzero centers M_{01} and M_{02} , and in both planes the phase trajectories attempt to adhere to the boundary of the region with zero effective energy, but in the final count they do not succeed in doing so. As a result, the cosmological acceleration executes anharmonic oscillations with large amplitude around the value $\Omega_0 = -1$. This case corresponds to the parameters listed in Eq. (14) and the initial conditions listed in Eq. (15) (see Figs. 23–25).

II. Rebound. The phase trajectories in the Σ_Φ plane tend asymptotically to the line $Z = 0$, whereas the phase trajectories in the Σ_φ plane are repulsed from the saddle points M_{01} and M_{02} and escape to infinity along the asymptote $\varphi = z, \tau \rightarrow \infty$. The cosmological acceleration after the burst enters the inflation regime – the model parameters listed in Eq. (10) and the initial conditions listed in Eq. (13) (see Figs. 20–22).

III. Adherence. The phase trajectories in both planes, Σ_Φ and Σ_φ , press down upon the zero effective energy hypersurfaces. This happens because of repulsion of the phase trajectory from a saddle point (See Fig. 7, for example) or because of attraction to an inaccessible center/focus. The effective energy falls rapidly to zero and the cosmological acceleration tends to $-\infty$ – a very rapid braking takes place: the parameters listed in Eq. (4) and the initial conditions listed in Eq. (7) (Figs. 7–10), the parameters listed in Eq. (10) and the initial conditions listed in Eq. (12) (see Figs. 17–19).

4 Some results of numerical modeling

4.1 Case of inaccessibility of the singular points M_{01} and M_{02}

$$\mathbf{P} = [1, -1, 1, -1, 1, 0]. \quad (10)$$

4.1.1 General properties of the phase space

In this case, the singular points have the same coordinates as in the previous case (5), but the invariant characteristics σ_i^2 are equal to

$$\sigma_1^2 = -\frac{3}{8}, \quad \sigma_2^2 = \frac{3}{8}, \quad \sigma_3^2 = 0.$$

The singular points M_{01} and M_{02} of the dynamical system are inaccessible.

4.1.2 Phase trajectories of the dynamical system

Figures 14–16 present results of numerical modeling of dynamical system (1) for the model parameters listed in Eq. (10) and the initial conditions listed in Eq. (11):

$$\mathbf{I} = [0.7, 0.5, 0.1, 0]. \quad (11)$$

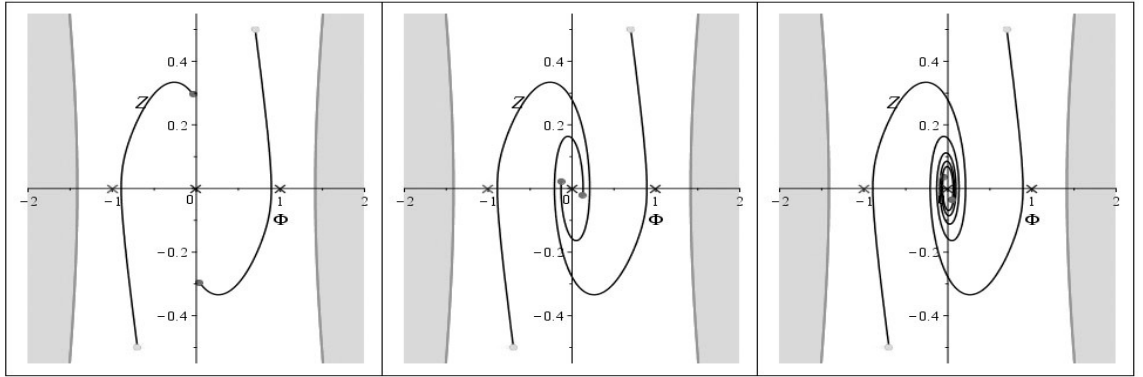


Figure 14: Cosmological evolution of a scalar doublet with the parameters listed in Eq. (10) and the initial conditions listed in Eq. (11) in the *classical* plane $\Sigma_\Phi \equiv \{\Phi, Z\}$. The phase diagrams correspond to the times (from left to right) $\tau = 5, 10$ and 20 .

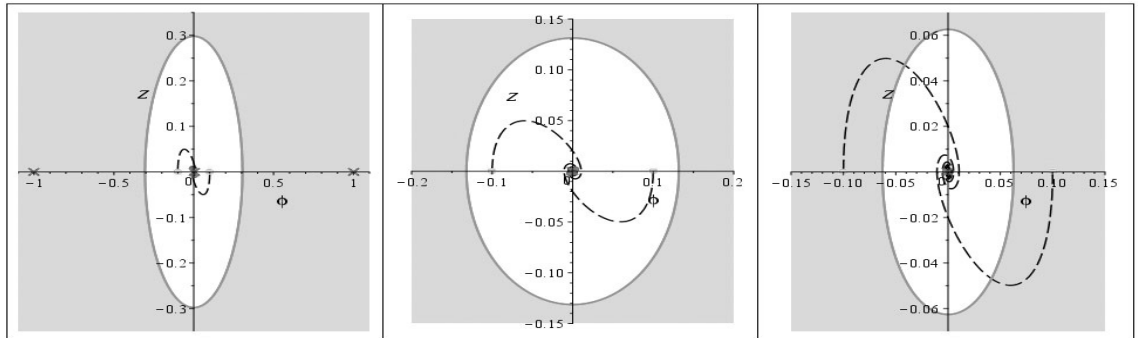


Figure 15: Cosmological evolution of a scalar doublet with the parameters listed in Eq. (10) and the initial conditions listed in Eq. (11) in the *phantom* plane $\Sigma_\varphi \equiv \{\varphi, z\}$. The phase diagrams correspond to the times (from left to right) $\tau = 5, 10$ and 20 .

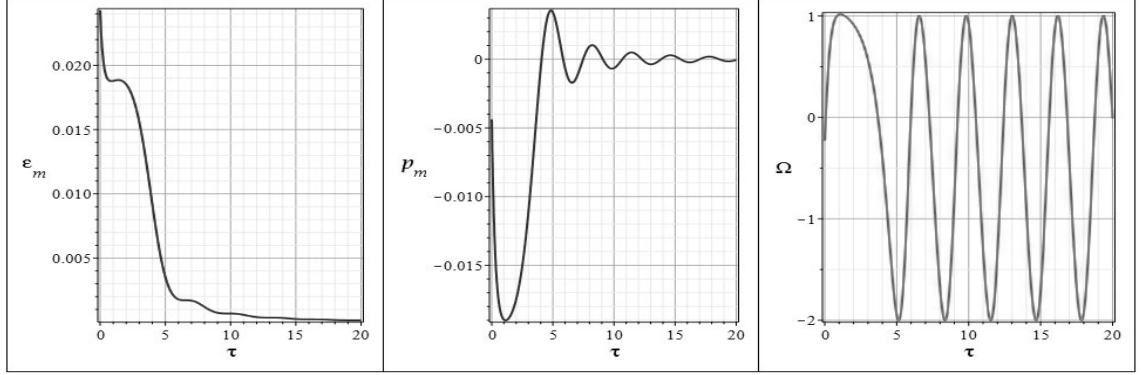


Figure 16: Cosmological evolution of the physical characteristics of the cosmological model with the parameters listed in Eq. (10) and the initial conditions listed in Eq. (11). From left to right: the dimensionless effective energy $\log(\mathcal{E})$, the dimensionless effective pressure $\text{Lig}(p_m)$, and the invariant cosmological acceleration $\text{Lig}(\Omega)$. The gray horizontal line in the last graph corresponds to the value $\Omega = 1$, i.e., to inflation.

Thus, for the initial conditions listed in Eq. (11), the phase trajectories of the dynamical system in both planes, Σ_Φ and Σ_φ , wind around and onto the zero center M_0 . Here the effective energy and pressure of the system tend to zero while the invariant cosmological acceleration executes oscillations around the value $\Omega = -1/2$ corresponding to the macroscopic nonrelativistic equation of state $\kappa = 0$. Precisely speaking, the same oscillations arise in the model with a classical scalar field (see [10, 11]). Figures 17–19 present results of numerical modeling of dynamical system (1) for the model parameters listed in Eq. (10) and the initial conditions listed in Eq. (12):

$$\mathbf{I} = [0.7, 0.5, 0.9, 0]. \quad (12)$$

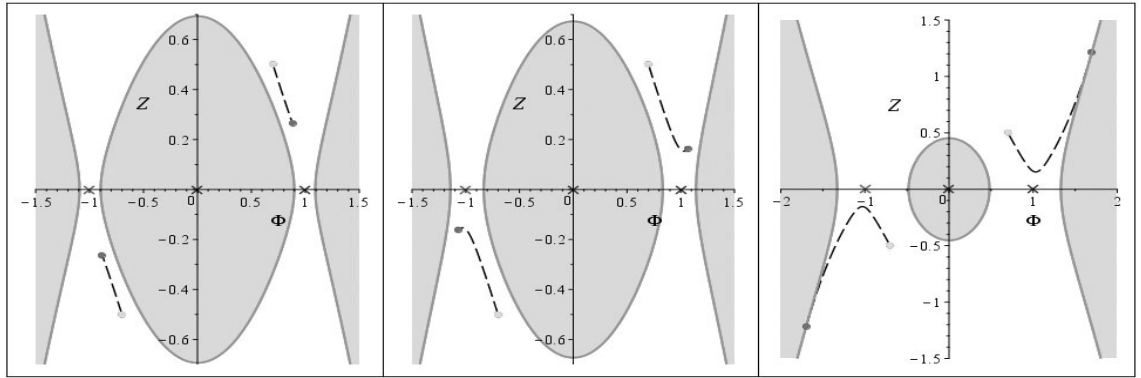


Figure 17: Cosmological evolution of a scalar doublet with the parameters listed in Eq. (10) and the initial conditions listed in Eq. (12) in the *classical* plane $\Sigma_\Phi \equiv \{\Phi, Z\}$. The phase diagrams correspond to the times (from left to right) $\tau = 0.5, 1.5$ and 2.99 .

Figures 20 and 21 present results of numerical modeling of dynamical system (1) for the model parameters listed in Eq. (10) and the initial conditions listed in Eq. (13):

$$\mathbf{I} = [0.7, 0.5, 1.5, 0], \quad (13)$$

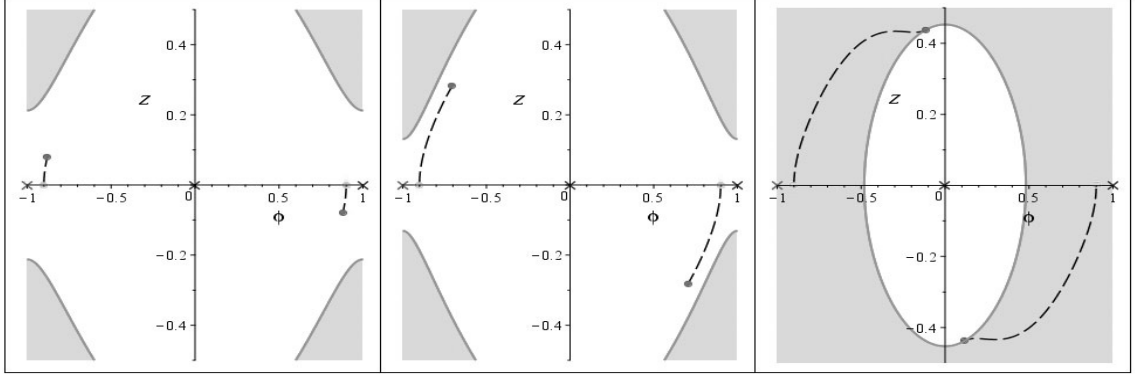


Figure 18: Cosmological evolution of a scalar doublet with the parameters listed in Eq. (10) and the initial conditions listed in Eq. (12) in the phantom plane $\Sigma_\varphi \equiv \{\varphi, z\}$. The phase diagrams correspond to the times (from left to right) $\tau = 0.5, 1.5$ and 2.99 .

when the dynamical system starts from a position higher than the singular point M_{01} . This case can be called a *rebound* – in the phantom plane the system rebounds from the forbidden region and rapidly grows the potential and kinetic energy of the phantom field, in the process entering the inflationary regime of acceleration.

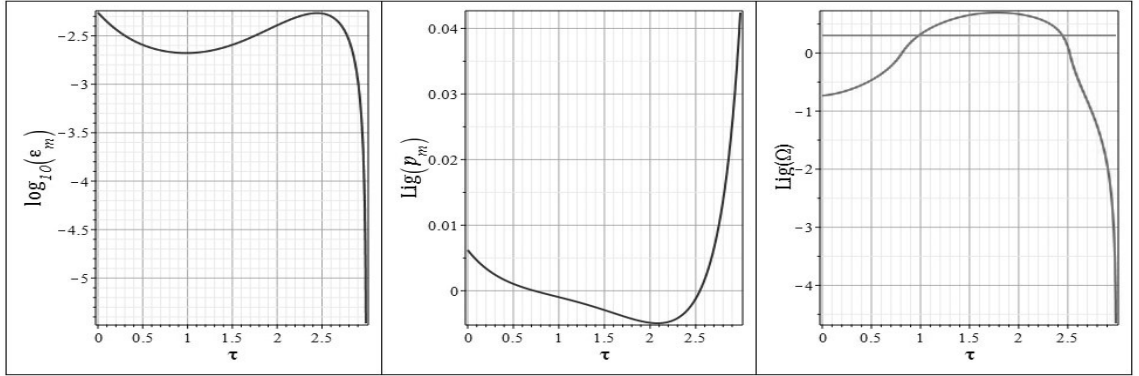


Figure 19: Cosmological evolution of the physical characteristics of the cosmological model with the parameters listed in Eq. (10) and the initial conditions listed in Eq. (12). From left to right: the dimensionless effective energy $\log(\mathcal{E})$, the dimensionless effective pressure $\text{Lig}(p_m)$, and the invariant cosmological acceleration $\text{Lig}(\Omega)$. The gray horizontal line in the last graph corresponds to the value $\Omega = 1$, i.e., to inflation.

Figure 22 depicts the evolution of the physical characteristics of the cosmological model with the parameters listed in Eq. (10) and the initial conditions listed in Eq. (13).

4.2 Case of inaccessibility of the singular points M_{10} and M_{20}

$$\mathbf{P} = [-1, 1, -1, 1, 1, 0]. \quad (14)$$

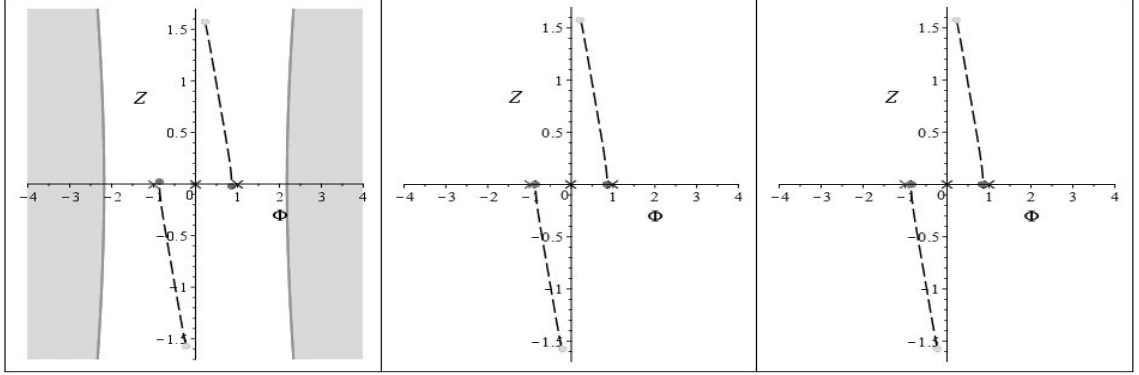


Figure 20: Cosmological evolution of a scalar doublet with the parameters listed in Eq. (10) and the initial conditions listed in Eq. (13) in the *classical* plane $\Sigma_\Phi \equiv \{\Phi, Z\}$. The phase diagrams corresponds to the times (from left to right) $\tau = 1, 5$ and 8.79 .

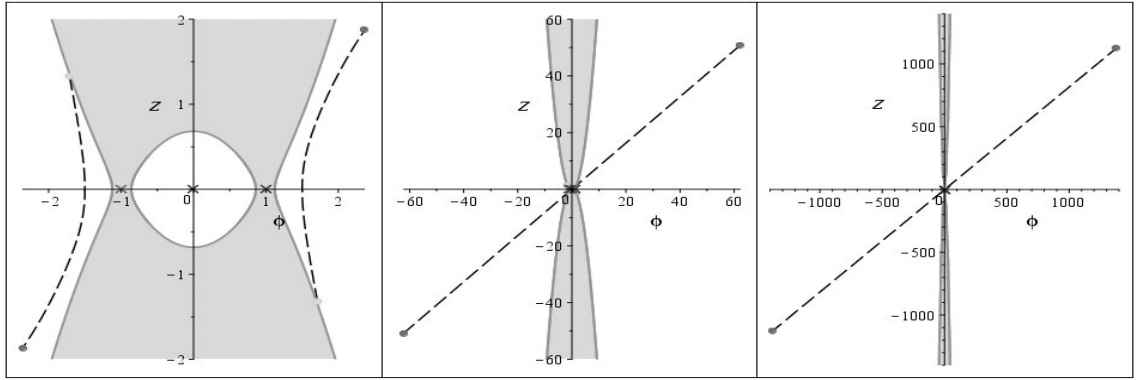


Figure 21: Cosmological evolution of a scalar doublet with the parameters listed in Eq. (10) and the initial conditions listed in Eq. (13) in the *phantom* plane $\Sigma_\varphi \equiv \{\varphi, z\}$. The phase diagrams corresponds to the times (from left to right) $\tau = 1, 5$ and 8.79 .

4.2.1 General properties of the phase space

In this case, the singular points have the same coordinates as in the previous case (5), and the invariant characteristics σ_i^2 are equal to

$$\sigma_1^2 = \frac{3}{8}, \quad \sigma_2^2 = -\frac{3}{8}, \quad \sigma_3^2 = 0.$$

The singular points M_{10} and M_{20} of the dynamical system are inaccessible.

4.2.2 Phase trajectories of the dynamical system

Figures 23–25 present results of numerical modeling of dynamical system (1) for the model parameters listed in Eq. (14) and the initial conditions listed in Eq. (15):

$$\mathbf{I} = [0.5, 0.5, 0.5, 0]. \quad (15)$$

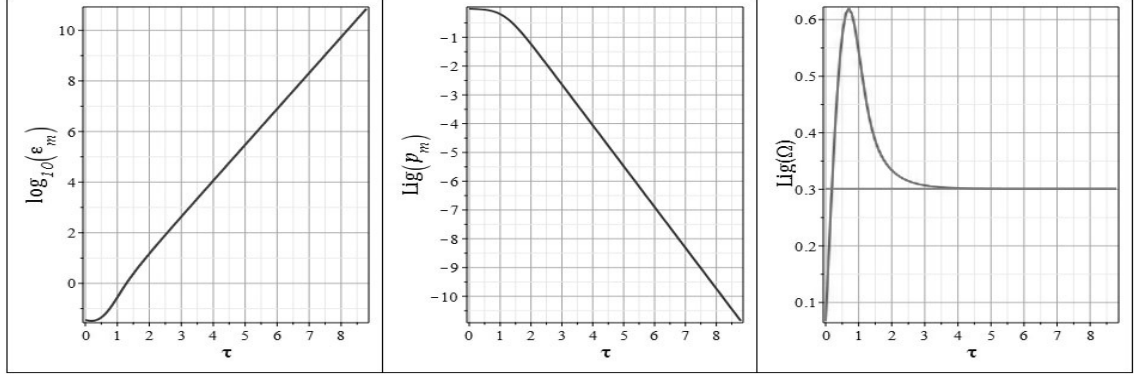


Figure 22: Cosmological evolution of the physical characteristics of the cosmological model with the parameters listed in Eq. (10) and the initial conditions listed in Eq. (13). From left to right: the dimensionless effective energy $\log(\mathcal{E})$, the dimensionless effective pressure $\text{Lig}(p_m)$, and the invariant cosmological acceleration $\text{Lig}(\Omega)$. The gray horizontal line in the last graph corresponds to the value $\Omega = 1$, i.e., to inflation.

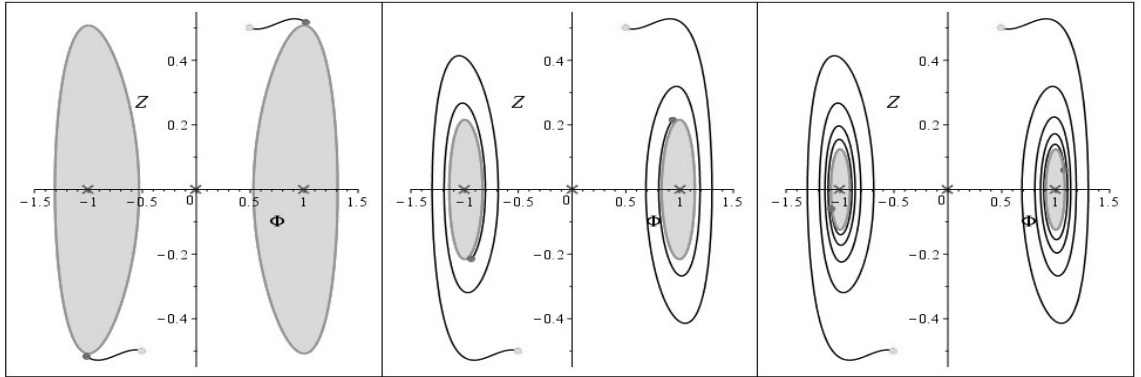


Figure 23: Cosmological evolution of a scalar doublet with the parameters listed in Eq. (14) and the initial conditions listed in Eq. (15) in the *classical* plane $\Sigma_\Phi \equiv \{\Phi, Z\}$. The phase diagrams correspond to the times (from left to right) $\tau = 5, 10$ and 20 .

It can be said that the behavior of the dynamical system has practically no dependence on the initial conditions despite the fact that the geography of the forbidden regions can be substantially different, which is probable evidence of stability of the behavior of the model for the parameters listed in Eq. (14) with respect to a change in the initial conditions. A study of the behavior of the dynamical system under an increase by a factor of 10 of the absolute values of the model parameters α_m and β_m , but with their signs left unchanged $\mathbf{P} = [10, -10, 1, -1, 1, 0]$, leads to qualitatively the same results with the one difference being that the amplitude of the oscillations of the cosmological acceleration decreases abruptly and is on the order of 1 (in Fig. 25 it exceeds 60).

5 Conclusions

Summarizing the results of the study presented here, we note that the peculiarities of dynamical system (1) revealed in this work are associated, first of all, with attraction of its phase trajectories to zero effective

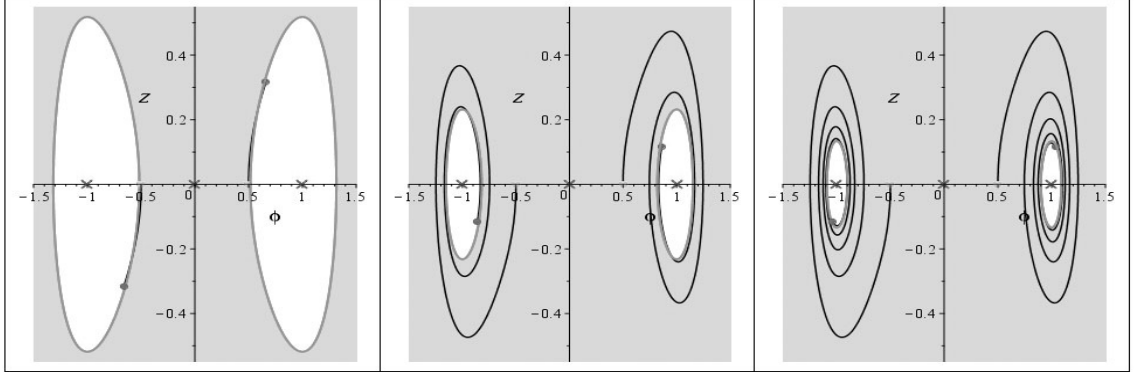


Figure 24: Cosmological evolution of a scalar doublet with the parameters listed in Eq. (14) and the initial conditions listed in Eq. (15) in the *phantom* plane $\Sigma_\varphi \equiv \{\varphi, z\}$. The phase diagrams correspond to the times (from left to right) $\tau = 5, 10$ and 20 .

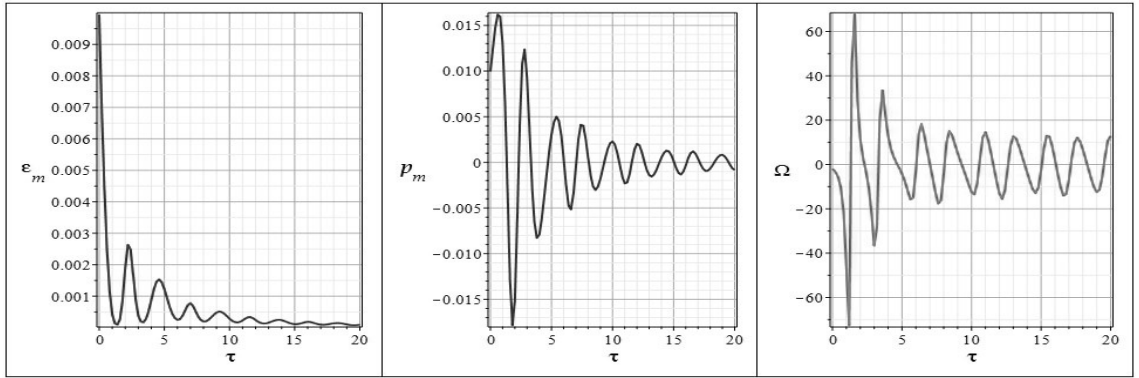


Figure 25: Cosmological evolution of the physical characteristics of the cosmological model with the parameters listed in Eq. (14) and the initial conditions listed in Eq. (15).

energy hypersurfaces and can form the basis of new cosmological scenarios. Indeed, the passage of the cosmological model to stationary orbits with zero effective energy for nonzero potentials of the scalar fields of an asymmetric doublet and their first derivatives allows us to treat these orbits as purely vacuum states of these fields, corresponding to zero curvature of Friedmann spacetime, i.e., to a purely Euclidean space. This space, as it turns out, can be non-empty and contain matter in the form of a pair of synchronously oscillating scalar fields, which can be considered as virtual vacuum fields. Note that all of the considered cases of adherence of the dynamical system to the zero effective energy surfaces correspond to very early stages of cosmological evolution. The possible instability of these scalar fields, stationary with respect to perturbations, can become a source of creation of real particles as a result of scalar interactions, not the result of a gravitational instability.

This work was performed within the scope of the Russian Government Program of Competitive Growth of Kazan Federal University.

References

- [1] Yu. G. Ignat'ev and I. A. Kokh, Russ. Phys. J., **61**, No. 6, 1079–1092 (2018).
- [2] Yu. G. Ignat'ev and I. A. Kokh, Russ. Phys. J., **61**, No. 9, 1590–1596 (2018).
- [3] Yu. G. Ignat'ev and I. A. Kokh, Russ. Phys. J., **62**, No. 2, in press (2019).
- [4] I.Ya. Aref'eva, N. V. Bulatov, R. V. Gorbachev, and S. Yu. Vernov, Class. Quantum Grav. – 2014. – V. **31**, 065007.
- [5] Yu. Ignat'ev, A. Agathonov, M. Mikhailov, and D. Ignatyev, Astr. Space Sci., **357**, 61 (2015).
- [6] Yurii Ignat'ev, Alexander Agathonov, and Dmitry Ignatyev, arXiv:1608.05020 [gr-qc] (2016).
- [7] Yu. G. Ignat'ev, A. A. Agathonov, and D. Yu. Ignatyev, Grav. Cosmol. – 2018. – V. **24**, 1, 1–12.
- [8] Yurii Ignat'ev, Alexander Agathonov, and Irina Kokh, arXiv:1810.09873 [gr-qc].
- [9] Yu. G. Ignat'ev and A. R. Samigullina, Space, Time and Fund. Interact., No. 1, 100–102 (2017).
- [10] Yu. G. Ignat'ev and A. R. Samigullina, Russ. Phys. J., **60**, 7, 1173–1181 (2017).
- [11] Yu. G. Ignat'ev, D. Yu. Ignatyev, and A. R. Samigullina, Grav. Cosmol., **24**, 2, 148–153 (2018); arXiv:1705.05000 [gr-qc].